Evolutionary Loss of Cone Photoreception in Balaenid Whales Reveals Circuit Stability in the Mammalian Retina

Lorian E. Schweikert[1], Jeffry I. Fasick[2*], Michael S. Grace[1*]

[1] Department of Biological Sciences, Florida Institute of Technology, Melbourne, FL 32901, USA.

[2] Department of Biological Sciences, The University of Tampa, Tampa, FL 33606, USA.

*Address correspondence and reprint requests to:

M. S. Grace, Department of Biological Sciences, Florida Institute of Technology, Melbourne, FL 32901; phone: 321-674-7573; FAX: 321-674-8864; email: mgrace@fit.edu

J. I. Fasick, Department of Biological Sciences, The University of Tampa, Tampa, FL 33606; phone: 813-257-3202; FAX: 813-258-7496; email: jfasick@ut.edu

Running Head: Effect of rod monochromacy on signaling pathways

Keywords: whale, rod monochromacy, opsin mutation, rod signaling, retinal organization, AB_2156055, AB_177457, AB_304300, AB_2253622, AB_141780, AB_143165

ABSTRACT

The classical understanding of mammalian vision is that it occurs through "duplex" retinae containing both rod and cone photoreceptors, the signals from which are processed through rod- and/or cone-specific signaling pathways. The recent discovery of rod monochromacy in some cetacean lineages provides a novel opportunity to investigate the effects of an evolutionary loss of cone photoreception on retinal organization. Sequence analysis of right whale (*Eubalaena glacialis;* family Balaenidae) cDNA derived from long-wavelength sensitive (LWS) cone opsin mRNA identified several mutations in the opsin coding sequence, suggesting the loss of cone cell function, but maintenance of non-photosensitive, cone opsin mRNA-expressing cells in the retina. Subsequently, we investigated the retina of the closely related bowhead whale (*Balaena mysticetus;* family Balaenidae) to determine how the loss of cone-mediated photoreception affects light signaling pathways in the retina. Anti-opsin immunofluorescence demonstrated the total loss of cone opsin expression in *B. mysticetus*, while light microscopy, transmission electron microscopy and bipolar cell (PKC-α and recoverin) immunofluorescence revealed the maintenance of cone soma, putative cone pedicles, and both rod and cone bipolar cell types. These findings present the first immunological and anatomical evidence of a naturally occurring rod-monochromatic mammalian retina, and suggest that despite the loss of cone-mediated photoreception, the associated cone signaling structures (i.e., cone synapses and cone bipolar cells) may be maintained for multi-channel rod-based signaling in balaenid whales.

INTRODUCTION

The retinae of nearly all vertebrate animals contain both rod and cone photoreceptor cells. These two cell types, which form the "duplex" retina, play distinct, yet complementary roles in visual function (Rodieck, 1973; Szel et al., 2000; Ahnelt and Kolb, 2000; Peichl, 2005). Rod photoreceptors support dim light (i.e., scotopic) vision because of their high sensitivity, while cone photoreceptors support vision in bright light (i.e., phototopic) conditions.

The signaling pathways of rod and cone photoreceptors and the architecture of the mammalian retina are well known (see Wässle, 2004 for review). Photoreceptors contain a light-sensitive outer-segment, an inner-segment, a nucleus-containing soma, and a synaptic end, known as a spherule in rods and a pedicle in cones. Typically, graded potentials from photoreceptors are relayed to bipolar cells and then to ganglion cells, the axons of which convey visual information to the brain. Retinal signaling of rods and cones, however, is more complex than two distinct pathways of information flow. Cone photoreceptors synapse directly onto two functionally distinct classes of cone bipolar cells (CBC), ON-CBCs and OFF-CBCs (Kolb and Nelson, 1995; Hartveit, 1997), whereas rod photoreceptors convey information to both rod bipolar cells (RBC; Devries and Baylor, 1995) and CBCs (Soucy et al., 1998; Tsukamoto et al., 2001). In fact, rods require CBCs in each of the three distinct rod signaling pathways through the retina (Sharpe and Stockman, 1999; Wässle, 2004). Rod photoreceptors and RBCs utilize the cone circuitry rather than communicating directly with the ganglion cell network, perhaps because (1) rods evolved after cone photoreceptors and are believed to have been integrated into the pre-existing cone circuitry (Masland, 2001) and (2) the widespread

cone circuitry and its complex secondary connections with amacrine and ganglion cells may help support higher order visual processes (e.g., direction selectivity, and center-surround receptive fields; Masland, 2001; Wässle, 2004) important in both scotopic and photopic conditions.

The reliance of rod photoreceptor signaling on cone photoreceptors and CBCs would seemingly make these cells indispensible in the mammalian retina (Peichl, 2005). Yet, the complete natural loss of cone photoreception has recently been described in some cetacean and xenarthran species (Meredith et al., 2013; Emerling and Springer, 2015). The genomic examination of cetacean opsins demonstrated the inactivation of the long-wavelength sensitive (LWS) cone opsin gene in five independent lineages (Meredith et al., 2013). This loss of the LWS cone opsin class, along with the pseudogenized short-wavelength sensitive (SWS) cone opsin gene of cetaceans (Fasick et al., 1998; Levenson and Dizon, 2003; Peichl et al., 2001), suggests that some whales are rod monochromatic – they have lost cone photoreception and retain only rod photoreceptors. This discovery raises two important questions pertaining to mammalian retinal organization: (1) have cone photoreceptors as cellular entities been lost, or do they simply lack functional opsins, and (2) is the retinal circuitry serving the cones (e.g., cone bipolar cells) maintained, or is it lost as a consequence of cone function loss? The latter would require modification of the rod signaling pathway, which usually feeds into the cone pathway to transmit rod signals to retinal ganglion cells.

We investigated the consequences of the loss of cone photoreception on the functional organization of the mammalian retina by examining retinal tissue of one cetacean clade (the family Balaenidae) that possess both LWS and SWS pseudogenes.

Genetic analyses were performed on the North Atlantic right whale (*Eubalaena glacialis*) in order to assess the effects of the mutation on LWS cone opsin gene expression, and histological and immunochemical analyses on the bowhead whale (*Balaena mystcetus*) in order to assess the effects of the mutation on the cellular architecture of the retina.

METHODS

Tissue Collection and Preparation

An eye (CALO 0901) was collected from a euthanized *E. glacialis* calf (approximately 2 yrs. old) after stranding on the east coast of Florida, and stored frozen at -80°C immediately following collection. A partial eyecup from a mature bowhead whale (*B. mysticetus*) was collected during the 2012 Nunavut bowhead whale hunt in Arctic Bay, Canada. The partial eyecup was fixed in 4% paraformaldehyde in 0.1 M phosphate buffered saline, pH 7.3 and partitioned so that both peripheral and central regions of the eyecup could be analyzed by histology and immunofluorescence. For comparative purposes, bovine (*Bos taurus*) eyes were collected immediately following euthanasia at a local abattoir. The eyes were enucleated and the vitreous humor removed prior to immersion of the eyecup in the appropriate fixative (see below). Left eyes were prepared for transmission electron microscopy and right eyes were prepared for immunofluorescence.

Gene Cloning and Sequencing

RNA extraction and first strand synthesis from *E. glacialis* retinal tissue was performed as described in Bischoff et al., (2012). In brief, total RNA was isolated from

thawed retinal tissue using the RiboPure 96 Kit (Applied Biosystems/Ambion, Austin, TX). First strand cDNA was generated from total RNA using an oligo dT_{18} primer and reverse transcriptase provided in a Reverse Transcription System kit (Promega, Madison, WI). The coding region of LWS opsin cDNA was isolated by polymerase chain reaction (PCR) using oligonucleotide primers designed to amplify exons 2-6 between coding nucleotide positions 115 and 1069. Sense and antisense primers annealing within exons 2 and 6, respectively, were designed based on consensus nucleotide sequences of previously published cetacean LWS opsins. The upstream sense oligonucleotide primer was 5'-CCTTCGACGGCCCCAATT-3'; the downstream antisense oligonucleotide primer was 5'-GATGAGGCCTCTGTTTTGGA-3'. Each amplification was carried out in a 50-µl mixture containing 0.2 µM of each primer, 2 µl of reverse transcribed single-stranded cDNA, and Amplitaq Gold master mix (Invitrogen, Carlsbad, CA). The thermal cycle parameters began with 95°C for 5 min, followed by 35 cycles consisting of 95°C for 1 min, 54°C for 1 min, 72°C for 1 min with a final 8 min incubation at 72°C. PCR products were sequenced directly with the final opsin cDNA sequence being based on consensus double-stranded sequences from at least two independent PCR amplifications. cDNA sequences were confirmed using National Center for Biotechnology Information (NCBI) blast and homology alignments with other vertebrate LWS opsin sequences.

Antibody Characterization

The primary antisera included in this study were used as tissue markers to indicate the morphology and distribution of target cells rather than to establish a novel and unique localization pattern of the antigens (Table 1). Non-specific labeling (i.e., labeling apart

from appropriate cell morphology) was not seen from any of the antibodies. The rhodopsin antibody (Millipore Cat# MAB5316, RRID:AB_2156055) appropriately stains photoreceptor outer segments in the vertebrate retina (Taylor et al., 2015). The cone opsin antibodies also appropriately stain photoreceptor outer segments in the vertebrate retina anti-LWS cone opsin (CERN 906, Taylor and Grace, 2005; Taylor et al., 2011), anti-cone opsin (CERN 874, Candal et al., 2005) and anti-SWS cone opsin (Millipore Cat# AB5407, RRID:AB_177457, Zeiss et al., 2011). Double labeling by cone opsin and rhodopsin antibodies of photoreceptor outer segments was never observed. The PKC alpha antibody (Abcam Cat# ab4127, RRID:AB_304300) labels an appropriate morphology for rod bipolar cells (Fernández-Medarde et al., 2009) while the recoverin antibody (Millipore Cat# AB5585, RRID:AB_2253622) labels an appropriate morphology for cone bipolar cells (Gargini et al., 2007) across the inner nuclear and inner plexiform layers of the retina. Controls for each specimen included omission of the primary antisera and single-labeling with each primary and secondary combination.

Immunofluorescence

Bovine and porcine eyecups were fixed in a solution of 4% paraformaldehyde and 15% picric acid in 0.1 M sodium phosphate buffer, pH 7.4. Following a minimum of 48 h of fixation, 8mm^2 patches of tissue were excised from the central and peripheral regions of the eyecup and infiltrated with 25% sucrose in 0.1 M Tris buffer, pH 7.4, then embedded in Tissue-Tek at -25°C. Frozen cross sections (20 µm thick) of bovine and *B. mysticetus* eyecups were were cut on a Leica CM1850 cryostat and thaw-mounted onto gelatin–coated glass microscope slides and dried at room temperature overnight. Slides

were then placed into fixative for 1h, followed by four, 15 min washes in Tris-buffered saline (0.5 M Trizma buffer, 0.9% NaCl, pH 7.4). Primary antisera were diluted in Tris-buffered saline containing 0.25% λ-carrageenan, 1% bovine serum albumin, and 0.3% Triton X-100, and applied to the slides for overnight incubation (minimum 8 h) at room temperature. After four, 15 min rinses in TBS, slides were incubated for 1 h at room temperature in fluorophore-conjugated secondary antisera. Following four rinses in Tris-buffered saline, slides were coverslipped with Slowfade Gold mounting medium with DAPI nucleic acid stain (Life Technologies, Grand Island, NY) and imaged using EZ-C1 software (MGH Confocal Microscope Core, RRID:SCR_009921) on a Nikon C1Si upright confocal laser-scanning microscope (Nikon Instruments, Melville, NY).

Photoreceptor subtypes were labeled using the anti-rhodopsin and either the anti-SWS cone opsin or one of the two anti-LWS cone opsin antisera. Primary antisera were labeled with secondary antisera that were conjugated to Alexa Fluor fluorescent dyes (Life Technologies Cat# A21424, RRID:AB_10566287; Life Technologies Cat# A11008, RRID:AB_10563748). Immunofluorescence was performed with bovine retina (positive control) and *B. mysticetus* retina concurrently. Photoreceptor densities (number per 25μm linear expanse of section) were counted manually, and photoreceptor widths and lengths were digitally measured using NIS Elements (NIS-Elements Basic Research, RRID:SCR_002776).

The *B. mysticetus* retina was immunolabeled using the anti-protein kinase C-alpha (PKCα) to identify RBCs, while CBCs were immunolabeled using the anti-recoverin. The secondary anti-rabbit antiserum was the same as described above. Bipolar cell types were identified and classified by their immunoreactivity and cell morphology,

particularly by the stratification level of their axon terminus in the inner plexiform layer (IPL).

Light Microscopy

For transmission light microscopy, bovine eyecups were fixed in a solution of 2.5% glutaraldehyde, 2.5% paraformaldehyde, and 0.008% $CaCl_2$ in 0.1 M sodium cacodylate, pH 7.4. Following 48 h of fixation, a 4x8 mm patch of tissue was excised from the periphery of the eyecup and rinsed in phosphate-buffered saline (0.9% NaCl, pH 7.4) prior to being dehydrated in a graded acetone series and embedded in Durcupan ACM epoxy resin (Electron Microscopy Sciences, Hatfield, PA). Retinal cross sections (1-µm thickness) of Durcupan-embedded material were cut with glass knives and heat-mounted onto glass slides. Sections were stained over heat with 1:1 mixture of 1% azure II in deionized water and 1% methylene blue in 1% sodium borate, and coverslipped with immersion oil. Images were taken with a Pixera Penguin 600CL camera on a Zeiss Axioskop2 light microscope.

Transmission Electron Microscopy

For transmission electron microscopy, bovine and *B. mysticetus* retinal tissue was processed as described above for light microscopy with the addition of a 2 hr incubation in 1% osmium tetroxide prior to plastic-embedding. Ultrathin, silver (*ca.* 30 nm thickness) retinal cross-sections were cut with a diamond knife on a Leica Ultracut UC6 ultramicrotome, then mounted on Formvar-coated copper 150 mesh grids, and stained in a CO_2-reduced environment with 5% aqueous uranyl acetate solution for 15 min followed

by 6% aqueous lead citrate for 5 min and a 5 min rinse in deionized water. Sections were imaged on a Zeiss EM900 transmission electron microscope (Carl Zeiss Inc., Peabody MA) at 50kV, and photographed using Olympus ITEM Software.

RESULTS

E. glacialis LWS cone opsin gene is transcribed in vivo

Extracted total retinal RNA was reverse transcribed to cDNA and then subjected to PCR in order to amplify coding regions of the LWS opsin transcript. Amplification of the full-length coding region was attempted using degenerate oligonucleotides based on homologous mammalian LWS opsin sequences, but failed to result in PCR products. Alternatively, we designed oligonucleotide primers based on homologous mammalian LWS opsin sequences which annealed within exons 2 and 6 in order to generate complete sequences for exons 3-5 as well as partial sequence for exons 2 and 6. We expected PCR amplification of *E. glacialis* retinal cDNA to result in a 954 bp band concurrent with the distance between the up- and down-stream primers in functional mammalian LWS coding sequences. Our PCRs resulted in a single truncated product of 786 base pairs. Sequence analyses of the PCR products revealed a sequence that had been spliced incorrectly in which exons 2, 3, 5 and 6 were retained intact with 96+% nucleotide identity to other cetacean LWS opsin sequences (Genbank accession # KU363818). . Exon 4, however, was missing from the *E. glacialis* LWS opsin cDNA sequence with exons 3 and 5 being spliced together at their respective intron/exon splice junctions. The remaining sequence (exons 5-6) of the *E. glacialis* LWS cone opsin identified here is identical to that of the Southern Atlantic right whale (*Eubalaena australis)* LWS cone

opsin sequence described by Meredith et al. (2013), except for two substitutions at deduced amino acid positions 251 and 252 with *E. glacialis* possessing the substitutions Gln for Glu and Lys for Glu, respectively. In functional LWS cone visual pigments these two substitutions occur in intracellular loop 3 of the opsin and, although quite distant from the protonated Schiff base to influence any kind of wavelength modulation, would influence the binding of G protein as well as arrestin.

LWS cone opsin protein is not expressed

To determine if LWS cone opsin is expressed in the Balaenid retina, we performed anti-opsin immunofluorescence in bowhead whale (*Balaena mysticetus*). Strong anti-rhodopsin immunofluorescence was observed in the rod outer segment (ROS) layer of the bowhead retina, but neither anti-LWS cone opsin labeling nor anti-SWS cone opsin labeling was observed (Fig.1 A–C). The retina of the bovine control, however, exhibited strong anti-rhodopsin labeling as well as strong labeling for both LWS and SWS cone opsin (Fig. 1D–F), with the density of SWS cone outer segments (COS) being less than that of LWS cones (~2:1 LWS:SWS; Table 2). The *B. mysticetus* ROS (19.72 ± 2.58 μm in length; 1.42 ± 0.20 μm in width) were densely packed (Table 2) and appeared similar in morphology to bovine ROS (11.86 ± 2.82 μm in length; 1.11 ± 0.1 μm in width). The outer segments of both bovine and *B. mysticetus* rods were slender relative to COS in bovine retina, and the SWS opsin-immunolabeled COS of the bovine retina were shorter than those of LWS cones (SWS cones: 8.57 ± 0.89 μm in length; 1.33 ± 0.18 μm in width; LWS cones: 8.98 ± 1.23 μm in length; 1.50 ± 0.20 μm in width). Labeling was not observed in control slides with omission of primary antibodies.

Cone photoreceptor outer and inner segments appear lost

To determine if the functional loss of cone photoreceptors by cone opsin mutation resulted in the loss of cone cells in the retina, light and transmission electron microscopy (TEM) was used to examine the photoreceptor mosaic of *B. mysticetus*. Light microscopy revealed only putative rod cells (Fig. 2A), with ROS that were morphologically uniform in length, width, and shape. In contrast, the bovine retinal photoreceptor layer contained morphologically distinguishable rod and cone outer segments; COS were conically-shaped and shorter in length than the cylindrical ROS (Fig. 2B). Because post-mortem tissue collection yielded whale retinal material that was unsuitable for ultrastructural examination of the outer segment disc membranes (which readily distinguishes rods from cones), we examined other morphologically distinguishing features of rods and cones – outer segment shape, outer segment length, mitochondrial density and inner segment vs. outer segment widths (Carter-Dawson and Lavail, 1979; Ahnelt and Kolb, 2000). Examination by TEM revealed a uniform photoreceptor layer characteristic of mammalian rod photoreceptor cells only, with no apparent COS or CIS (Fig. 2C,D), while the bovine retina had rod and cone photoreceptor cells that were readily distinguishable (Fig. 2E,F). Bovine rod photoreceptors had cylindrical outer segments of greater diameter than their inner segments, and a mitochondrial density similar to that of *B. mysticetus* rod photoreceptors (Fig. 2D,F). Bovine COS were shorter than ROS, conically-shaped, and of smaller diameter than their inner segments, and CIS exhibited more densely packed mitochondria than rod inner segments (Fig. 2E). The photoreceptor cells of *B. mysticetus* were all

similar to bovine rods, with cylindrical outer segments that were greater in diameter than their inner segments, and a lower density of mitochondria relative to bovine cones; no cone-like outer segments were observed (Fig. 2D,E).

Cone photoreceptor somata and pedicles are maintained

Although no evidence of COS or cone inner segments (CIS) was found in the *B. mysticetus* retina, cone cell nuclei and putative cone synaptic pedicles were easily identified by light and transmission electron microscopy. Cone photoreceptor nuclei were identified as the large entities in the outermost region of the outer nuclear layer (ONL; Fig. 3A); they were larger than rod nuclei and exhibited irregular clumping of heterochromatin. In the outer plexiform layer (OPL; photoreceptor synaptic layer) of the *B. mysticetus* retina, rod photoreceptor spherules and putative cone pedicles were identified morphologically (Fig.3A–C). Rod spherules were spherical in shape and smaller in size than cone pedicle-like profiles that were broad and appeared triangular in shape. Examination of the *B. mysticetus* retina by TEM revealed rod and cone photoreceptor nuclei, rod spherules and putative cone pedicles consistent with those observed by light microscopy (Fig. 3D–F).

Rod bipolar and cone bipolar cell populations are maintained

To determine the effect of the loss of cone photoreception on the associated cone signaling cells and retinal architecture in *B. mysticetus*, we examined bipolar cell populations utilizing RBC and CBC immunoreactivity. The *B. mysticetus* retina showed both anti-PKCα labeling (presumptive RBCs) and anti-recoverin labeling (presumptive

CBCs) of cell bodies in the inner nuclear layer (INL), dendritic terminals in the outer plexiform layer (OPL), and axon terminals in the inner plexiform layer (IPL; Fig. 4A,B).

Anti-PKCα immunolabeling of axonal terminals appeared across two strata in *B. mysticetus* retina: one at the border of the ganglion cell layer (GCL), as expected, and a second immediately superior as shown in figure 4A. This labeling pattern indicates either the immunolabeling of a CBC subtype in addition to RBCs or more likely, a bistratified RBC morphology. Nevertheless, *B. mysticetus* retinal bipolar cells that were fully PKCα-immunolabeled exhibited the characteristic morphology of mammalian RBCs (Fig. 4C, Table 3). *B. mysticetus* RBC somata were localized to the outermost part of the INL and projected long axons into the IPL terminating with bulbous dendrites adjacent to the GCL (Fig. 4C).

Anti-recoverin labeling of the *B. mysticetus* retina revealed cells with characteristics typical of mammalian CBCs (Fig. 4B, Table 3). Immunolabeled CBC dendrites terminated in both the inner half and in the outer half of the IPL, suggesting the labeling of OFF- and ON-CBCs respectively (Fig. 4D, OFF; 4E, ON). OFF-CBCs were localized to the inner part of the INL layer, and projected short axons terminating in the outer half of the IPL (Fig. 4D), while the labeled somata of ON-CBCs were in the outer portion of the INL with axons projecting into the inner half of IPL (Fig. 4E), but immediately superior to the GCL.

DISCUSSION

Here we describe for the first time how the evolutionary loss of cone photoreception affects the functional architecture of the mammalian retina. The results

presented here show that balaenid whale retinal circuitry remains largely intact following the total loss of cone photoreception. Our observations suggest that a natural, clade-wide loss of functional cone opsin does not disrupt the maintenance of cone synapses and cone bipolar cells to support rod-based signaling in the balaenid retina.

Meredith et al., (2013) utilized genomic DNA sequences to report inactivation mutations in the LWS cone opsin genes in the ancestral lineage of the cetacean family Balaenidae, which includes right and bowhead whales, as well as members of the following cetacean clades: Balaenopteroidea (rorquals and gray whale), Mesoplodon (*Mesoplodon bidens*, Sowerby's beaked whale), and Physeteridae (*Physeter microcephalus*, giant sperm whale; *Kogia breviceps*, pygmy sperm whale). Unlike Meredith et al. (2013), we utilized total retinal RNA from *E. glacialis* as template for LWS opsin sequence analyses. Our results show that LWS cone opsin is transcribed in retinal tissue, however the transcript is improperly spliced which would result in a truncated, nonfunctional opsin protein.

We examined the *B. mysticetus* retina by anti-opsin immunofluorescence in order to determine if cone opsin protein is expressed. We used a close relative of *E. glacialis, B. mysticetus,* for immunofluorescence studies due to inability to obtain appropriately preserved *E. glacialis* tissue. Two polyclonal LWS cone opsin antisera that produced strong immunolabeling of COS in the bovine retina failed to label the *B. mysticetus* retina. The absence of LWS opsin labeling in the *B. mysticetus* retina suggests that either the LWS opsin transcript is not expressed or that expressed, truncated LWS opsin protein is degraded rapidly upon synthesis. As expected, the SWS cone opsin protein was also absent from the bowhead retina due to complete inactivation of the gene and subsequent

loss of the photoreceptor class (Fasick et al., 1998; Levenson and Dizon, 2003; Peichl et al., 2001). The deactivation mutations observed in cetacean cone opsins along with the apparent loss of cone opsin expression seen here indicates the loss of cone photoreceptor function in the balaenid retina, providing the first histological evidence of a mammalian rod-monochromatic taxon. The presence of truncated LWS cone opsin mRNA, however, suggests that non-photoreceptive cone cells are retained in the balaenid whale retina.

Histological and ultrastructural examinations of the *B. mysticetus* retina indicate the loss of COS and CIS, but maintenance of cone somata and putative cone pedicles. The photoreceptor layer of the retina appeared to be only a uniform layer of ROS and RIS that possess the four morphological characteristics of mammalian rod photoreceptors: cylindrically-shaped outer segments, wider outer segments than inner segments, relatively long outer segment length, and low mitochondrial density relative to bovine cone photoreceptors (Carter-Dawson and Lavail, 1979; Ahnelt and Kolb, 2000). By comparison, rod and cone photoreceptors were morphologically distinguishable in the bovine retina examined here, as they are in the retina of another cetacean species, the long-finned pilot whale retina, *Globicephala melas* (Peichl et al., 2001), that has retained its LWS cone opsin gene (Meredith et al., 2013). Thus, it appears that COS have been lost in the *B. mysticetus* retina, which is a common downstream effect of photoreceptor gene mutations seen in various models of retinal pathology. Previous studies of photoreceptor gene defects on retinal organization show that mutations resulting in the functional loss of an entire photoreceptor type (rod or cone) can cause a pathological cascade of retinal degeneration and remodeling (Jones et al., 2002; Jones et al., 2003; Jones and Marc, 2005). The pathogenesis of these mutation-

based retinal dystrophies includes degeneration of the affected photoreceptor outer segment almost without exception (Jones et al., 2003; Marc et al., 2003; Strettoi et al., 2003). In retinitis pigmentosa, for example, a rod opsin gene mutation leads to rod outer segment loss, and in advanced stages, cone photoreceptor loss and progressive, global retinal degeneration (Milam et al., 1998). Here, widespread degeneration of retinal circuits was not observed, but atrophy of the non-functional cone outer segments of the *B. mysticetus* retina appeared to occur.

Despite the loss of COS, the conservation of cone photoreceptor nuclei and cone synaptic pedicles in the *B. mysticetus* retina may indicate retention of function of these cells. In some pathological models, photoreceptor somata can maintain normal synaptic connectivity even after loss of their inner and outer segments, (Jansen and Sanyal, 1984). In fact, clinical studies of human rod monochromats show that rod signals associated with rod-to-cone pedicle signaling are maintained, suggesting that cone somata continue to function as signal conduits despite loss of their own photoreceptive function (Stockman et al., 1995). *B. mysticetus* cone somata and synapses may be maintained for rod-to-cone pedicle signaling, as well as for signaling directly onto the bipolar cell network. Cone cell signaling is maintained in other mammals experiencing important changes in their photoreceptors. In hibernating ground squirrels, for example, a variety of retinal changes take place including "deconstruction" of cone outer segments, mitochondria in cone elipsoids, and cone ribbon synapses (for review, see Merriman et al., 2016), but these changes have little effect on cone synaptic communication (Mehta et al., 2013). In the experimentally detached retina of the domestic cat, while rods undergo reconfiguration of

their synapses and withdrawal of their axons, apparently normal cone synapses can be maintained (Fisher et al., 2005).

In *B. mysticetus*, retention of cones without outer segments corresponds with conservation of both CBC subtypes. In most mammals, RBCs, ON-CBCs, and OFF-CBCs are distinguishable from each other based upon the position of their cell somata in the INL and the stratification level of their axons in the IPL. RBC axons terminate at the border between the IPL and the GCL, while ON-CBC axons terminate in the inner half of the IPL and OFF-CBC axons terminate in the outer half of the IPL (Boycott and Wässle, 1991; Euler and Wässle, 1995; Wu et al., 2000. Wässle et al., 2009). To our knowledge, until now bipolar cell subtypes have not been described in rod monochromatic retinae. Here we show that in *B. mysticetus,* characteristic RBCs immunolabeled with PKC-α but not recoverin have terminals that project through the IPL, ramifying adjacent to the GCL. These *B. mysticetus* RBCs have a bistratified morphology that is unusual for mammals, but has been observed in the microbat *Carollia perspicillata* (Müller et al., 2013). Unlike *B. mysticetus*, microbats have functional cone photoreceptors (Müller and Peichl, 2005), but *C. perspicillata's* nocturnal behavior likely places particular importance on rod-based vision. The bistratified morphology of RBCs in microbats and *B. mysticetus* may indicate more complex processing of rod photoreceptor signals in these retinae (Müller et al., 2013).

A second bipolar cell population was immunolabeled with recoverin in the *B. mysticetus* retina, but not PKC-α. The axons of these recoverin-labeled cells projected to either the inner half or the outer half of the IPL, characteristic of ON- and OFF-CBCs, respectively. The integrity of the dendrites of both ON- and OFF-CBCs in the outer

plexiform layer suggests their activation by photoreceptor cells (Strettoi and Pignatelli, 2000; Marc et al., 2003). Thus in the *B. mysticetus* retina, CBCs likely receive signals either directly from rod photoreceptors or indirectly from rods *via* cone somata, or both.

Why are cone somata and CBCs maintained in a rod-monochromatic retina? In duplex vertebrate retinae, three distinct rod signaling pathways all utilize CBCs for signal transmission to ganglion cells, including one pathway that transmits signals *via* cone photoreceptor pedicles directly (Sharpe et al., 1989; Sharpe and Stockman, 1999). These multiple pathways increase the signaling speed and sensitivity range of rod-based vision (Sharpe and Stockman, 1999). The classical rod signaling pathway is the most light-sensitive, with rods synapsing directly onto RBCs and indirectly onto CBCs *via* amacrine cells to convey information to ganglion cells (Devries and Baylor, 1995). Rods also synapse directly onto cone pedicles (i.e., rod-cone coupling), which synapse on CBCs, which in turn convey information to ganglion cells (Sharpe et al., 1989; Sharpe and Stockman, 1999), creating a lower-sensitivity pathway which functions at brighter (i.e., mesopic) light intensities (Sharpe et al., 1989; Sharpe and Stockman, 1999). In a third pathway, rods synapse directly onto CBCs (Soucy et al., 1998; Hack et al., 1999; Tsukamoto et al., 2001). Direct synaptic connectivity of rods to CBCs underlies important aspects of retinal organization and function regardless of light intensity, such as center-surround receptive field organization and direction selectivity (Masland, 2001; Wässle, 2004). Thus, maintenance of cone somata and CBCs in the rod-monochromatic balaenid whale retina may provide a broader range of absolute sensitivity than possible with only RBCs (Fig. 5).

Examples of rod monochromacy have been described previously in amphibians and deep-sea fishes (Partridge et al., 1989; O'Brien et al., 1997; Bozzano et al., 2001; Kos et al., 2001; Mohun et al., 2010; Lisney et al., 2012), and more recently in mammals (Meredith et al, 2013; Emerling and Springer 2015). Meredith et al., (2013) postulated that SWS and LWS cone opsins have undergone convergent pseudogenization in multiple cetacean lineages perhaps to reduce noise caused by the cone visual system in dim light conditions. In addition, these authors suggest that rod monochromacy in whales may support improved scotopic vision and contrast detection for targeting prey. The rod density of *B. mysticetus* reported here (191,333 rods per mm^{-2}) falls within the range of rod monochromatic fishes (i.e., 180,000 to 250,000 per mm^{-2}; Wagner et al., 1998). However, rod photoreceptor density in the balaenid whale retina is dramatically lower than in some other dim-light-active vertebrate animals. Most mammals have a rod density range of 200,000 to 400,000 mm^2 (Peichl, 2005), while strictly nocturnal mammals (such as the African pouched rat) can have rod densities of 390-730,000 rods/mm^2 (Peichl and Moutairou, 1998). Based upon these observations, it appears that photoreceptor densities in rod monochromatic balaenid whale and deep-sea marine fish are lower than what might be predicted.

The results of this study show that the balaenid whale retina, despite loss of all COS and CIS, maintains otherwise normal retinal architecture including ON- and OFF-CBCs, and cone synapses as well. The conservation of cone synpases and cone bipolar cells may serve multi-channel, rod-based signaling in balaenid whales allowing for greater sensitivity across a broader range of light intensities than would be possible through rod-to-RBC signaling alone. These results suggest that the duplex organization of

the vertebrate retina exists not only to support rod- and cone-mediated photoreception, but provides multi-channel processing of the rod-based visual system for enhanced utility under a variety of lighting conditions.

ACKNOWLEDGEMENTS

We acknowledge the following individuals and funding sources for collection of the CALO 0901 eye: William McLellan, U. North Carolina (UNC) Wilmington; Craig Harms, Chris Butler, and Eric Anderson, North Carolina State U. Center for Marine Science and Technology; Gretchen Lovewell, National Marine Fisheries Service (NMFS); and Susan Barco, Virginia Aquarium. Tissue was collected under permit to Teri Rowles, NMFS. We would like to thank the Inupiat whale hunters of the Barrow Whaling Captains Association and the Alaska Eskimo Whaling Commission for their cooperation and allowing us to examine their whales and collect tissues. Hans Thewissen, J. Craig George and T. Sformo collected the retinal tissues from the landed whales at Barrow with the assistance of whaling crew members. Specimens were collected under NOAA NMFS Marine Mammal Permit #17350-00. We thank Ernst Peebles, University of South Florida (USF) St. Petersburg, for opening his laboratory to J.I.F. Funding for stranding response and necropsy was provided under Right Whale Necropsy Response Contract #EM133F07SE333323 to Michael Moore, Woods Hole Oceanographic Institution and William McLellan, UNC Wilmington, NMFS. We acknowledge T. Greco, College of Marine Science, USF St. Petersburg, for his assistance with electron microscopy, and G. Duncombe, Florida Institute of Technology (FIT), for assistance with confocal microscopy. We also thank Patrick Scott (Insight Vision

Center), Leo Peichl (Max-Planck-Institut für Hirnforschung), and Kristin Kopperud (FIT) for critical insight and helpful discussion. This work was supported in part by the Consortium for Wildlife Bycatch Reduction, New England Aquarium under NOAA Award #NA09NMF4520413 contractual to J.I.F., by NSF grant #DBI 0722570 to M.S.G., and by an NSF Graduate Research Fellowship to L.E.S.

Conflicts of Interest Statement

The authors verify that they have no conflicts of interest with other people or organizations that could inappropriately influence this work.

Authors Contributions to the Work

All authors had full access to all the data in the study and take responsibility for the integrity of the data and the accuracy of the data analysis. Study concept and design: JIF and MSG. Acquisition of Data: JIF and LES. Analysis and Interpretation of Data: JIF, MSG, and LES. Drafting of the Manuscript: LES. Obtained Funding: JIF. Administrative, technical, and material support: MSG and LES.

CITATIONS

Ahnelt P, Kolb H. 2000. The mammalian photoreceptor mosaic-adaptive design. Prog Retin Eye Res 19:711–777.

Bischoff N, Nickle B, Cronin, T, Velasquez S, Fasick J. 2012. Deep-sea and pelagic rod visual pigments identified in the mysticete whales. Vis Neurosci 29:95–103.

Boycott B, Wässle H. 1991. Morphological classification of bipolar cells of the primate retina. Eur J Neurosci 3:1069–1088.

Bozzano A, Murgia R, Vallerga, Hirano J, Archer S. 2001. The photoreceptor system in the retinae of two dogfishes, *Scyliorhinus canicula* and *Galeus melastomus*: possible relationship with depth distribution and predatory lifestyle. J Fish Biol 59:1258–1278.

Candal E, Anadón R, DeGrip W, Rodríguez-Moldes I. 2005. Patterns of cell proliferation and cell death in the developing retina and optic tectum of the brown trout. Dev Brain Res 154:101–119.

Carter-Dawson L, Lavail M. 1979. Rods and cones in the mouse retina. I. Structural analysis using light and electron microscopy. J Comp Neurol 188:245–262.

DeVries S, Baylor D. 1995. An alternative pathway for signal flow from rod photoreceptors to ganglion cells in mammalian retina. Proc Natl Acad Sci USA 92:10658–10662.

Emerling C, Springer M. 2015. Genomic evidence for rod monochromacy in sloths and armadillos suggests early subterranean history for Xenarthra. Proc R Soc Lond [Biol] 282:20142192.

Euler T, Wässle H. 1995. Immunocytochemical identification of cone bipolar cells in the rat retina. J Comp Neurol 361:461–478.

Fasick, J, Cronin T, Hunt D, Robinson P. 1998. The visual pigments of the bottlenose dolphin (*Tursiops truncatus*). Vis Neurosci 15:643–651.

Fernández-Medarde A, Barhoum R, Riquelme R, Porteros A, Núñez A, De Luis A, De Las Rivas J, De La Villa P, Varela-Nieto I, Santos E. 2009. RasGRF1 disruption causes retinal photoreception defects and associated transcriptomic alterations. J Neurochem 110:641–652.

Fisher SK, Lewis GP, Linberg KA, Verardo MR. 2005. Cellular remodeling in mammalian retina: results from studies of experimental retinal detachment. Prog Retinal Eye Res 24:395–431.

Gargini C, Terzibasi E, Mazzoni F, Strettoi E. 2007. Retinal organization in the retinal degeneration 10 (rd10) mutant mouse: a morphological and ERG study. J Comp Neurol 500:222–238.

Hartveit E. 1997. Functional organization of cone bipolar cells in the rat retina. J Neurophysiol 77:1716 –1730.

Jansen H, Sanyal S. 1984. Development and degeneration of retina in rds mutant mice: Electron microscopy. J Comp Neurol 224:71–84.

Jones B, Chen C, Watt C, Frederick J, Huang W, Baehr W, Marc R. 2002. Severe remodeling of the mouse neural retina triggered by rod degeneration. Invest Ophth Vis Sci 43:1885.

Jones B, Watt C, Frederick J, Baehr W, Chen C, Levine E, Milam A, LaVail M, Marc R, 2003. Retinal remodeling triggered by photoreceptor degenerations. J Comp Neurol 464:1–16.

Jones B, Marc R. 2005. Retinal remodeling during retinal degeneration. Exp Eye Res 81:123–137.

Kolb H, Nelson R. 1995. The organization of photoreceptor to bipolar synapses in the outer plexiform layer. In: Neurobiology and clinical aspects of the outer retina (Djamgoz MBA, Archer SN, Vallerga S, eds), pp 273–296. London: Chapman and Hall.

Kos M, Bulog B, Szél Á, Röhlich P. 2001. Immunocytochemical demonstration of visual pigments in the degenerate retinal and pineal photoreceptors of the blind cave salamander (*Proteus anguinus*). Cell Tissue Res 303:15–25.

Levenson D, Dizon A. 2003. Genetic evidence for the ancestral loss of short-wavelength-sensitive cone pigments in mysticete and odontocete cetaceans. Proc R Soc Lond B Biol Sci 270:673-679.

Lisney T, Theiss S, Collins S, Hart N. 2012. Vision in elasmobranchs and their relatives: 21st century advances. J Fish Biol 80: 2024–2054.

Marc R, Jones B, Watt C, Strettoi E. 2003. Neural remodeling in retinal degeneration. Prog Retin Eye Res 22:607–655.

Masland R. 2001. The fundamental plan of the retina. Nature Neurosci 4:877-886.

Meredith R, Gatesy J, Emerling C, York V, Springer M. 2013. Rod monochromacy and the coevolution of cetacean retinal opsins. PLoS Genet 9:e1003432.

Mehta B, Snellman J, Chen S, Li W, Zenisek D. 2013. Synaptic ribbons influence the size and frequency of miniature-like evoked postsynaptic currents. Neuron 77:516-527.

Merriman DK, Sajdek BS, Li W, Jones BW. 2016. Seasonal and post-trauma remodeling in the cone-dominant ground squirrel retina. Exp Eye Res http://dx.doi.org/10.1016/j.exer.2016.01.011

Milam A, Li Z, Fariss R. 1998. Histopathology of the human retina in retinitis pigmentosa. Prog Retin Eye Res 17:175-206.

Mohun S, Davies W, Bowmaker J, Pisani D, Himstedt W, Gower D, Hunt D, Wilkinson M. 2010. Identification and characterization of visual pigments in caecilians (Amphibia: Gymnophiona), an order of limbless vertebrates with rudimentary eyes. J Exp Biol 213:3586–3592.

Müller B, Peichl L. 2005. Retinal cone photoreceptors in microchiropteran bats. Invest Ophthalmol Vis Sci 46:2259–2259.

Müller B, Butz E, Peichl L, Haverkamp S. 2013. The rod pathway of the microbat retina has bistratified rod bipolar cells and tristratified AII amacrine cells. J Neurosci 33:1014–1023.

O'Brien J, Ripps H, Al-Ubaidi M. 1997. Molecular cloning of a rod opsin cDNA from the skate retina. Gene 193:141–150.

Partridge J, Shand J, Archer S, Lythgoe J, van Groningen-Luyben W. 1989. Interspecific variation in the visual pigments of deep-sea fishes. J Comp Physiol A 164:513–529.

Peichl L. and Moutairou K. 1998. Absence of short-wavelength sensitive cones in the retinae of seals (Carnivora) and African giants rats (Rodentia). Eur J Neurosci 10:2586-2594.

Peichl L, Behrmann G, Kröger R. 2001. For whales and seals the ocean is not blue: a visual pigment loss in marine mammals. Eur J Neurosci 13:1520–1528.

Peichl L. 2005. Diversity of mammalian photoreceptor properties: adaptations to habitat and lifestyle? Anat Rec A Discov Mol Cell Evol Biol 287:1001–1012.

Rodieck R. 1973. The vertebrate retina: Principles of structure and function. Oxford, England: W. H. Freeman

Sharpe L, Stockman A, MacLeod D. 1989. Rod flicker perception: scotopic duality, phase lags and destructive interference. Vision Res 29:1539–1559.

Sharpe L, Stockman A. 1999. Rod pathways: the importance of seeing nothing. Trends Neurosci 22:497–504

Stockman A, Sharpe L, Rüther K, Nordby K. 1995. Two signals in the human rod visual system: a model based on electrophysiological data. Vis Neurosci 12:951–970.

Strettoi E, Pignatelli V. 2000. Modifications of retinal neurons in a mouse model of retinitis pigmentosa. Proc Natl Acad Sci 97:11020–11025.

Strettoi E, Pignatelli V, Rossi C, Porciatti V, Falsini B. 2003 Remodeling of second-order neurons in the retina of rd/rd mice. Vision Res 43:867–877

Soucy E, Wang Y, Nirenberg S, Nathans J, Meister M. 1998. A novel signaling pathway from rod photoreceptors to ganglion cells in mammalian retina. Neuron 21:481–493.

Szél A´, Lukáts A, Fekete T, Szepessy Z, Ro¨hlich P. 2000. Photoreceptor distribution in the retinas of subprimate mammals. J Opt Soc Am A 17:568–579.

Taylor S, Grace M. 2005. Development of retinal architecture in the elopomorph species *Megalops atlanticus*, *Elops saurus* and *Albula vulpes* (Elopomorpha: Teleostei) Contrib Mar Sci 37:1–29.

Taylor S, Loew E, Grace M. 2011. Developmental shifts in functional morphology of the retina in Atlantic tarpon, Megalops atlanticus (Elopomorpha: Teleostei) between four ecologically distinct life-history stages. Vis Neurosci 28:309–323.

Taylor S, Loew E, Grace M. 2015. Ontogenic retinal changes in three ecologically distinct elopomorph fishes (Elopomorpha: Teleostei) correlate with light environment and behavior. Vis Neurosci 32:E005

Tsukamoto Y, Morigiwa K, Ueda M, Sterling P. 2001. Microcircuits for night vision in mouse retina. J Neurosci 21:8616–8623.

Wagner H, Fröhlich E, Negishi K, Collin S. 1998. The eyes of deep-sea fish II. Functional morphology of the retina. Prog Retin Eye Res 17:637–685.

Wässle H. 2004. Parallel processing in the mammalian retina. Nature Rev Neurosci 5:747–757.

Wässle H, Puller C, Müller F, Haverkamp S. 2009. Cone contacts, mosaics, and territories of bipolar cells in the mouse retina. J Neurosci 29:106–117.

Wu S, Gao F, Maple B. 2000. Functional architecture of synapses in the inner retina: segregation of visual signals by stratification of bipolar cell axon terminals. J Neurosci 20:4462–4470.

Zeiss C, Schwab I, Murphy, Dubielzig R. 2011. Comparative retinal morphology of the platypus. J Morphol 272:949–957.

FIGURE LEGENDS

Figure 1. Anti-opsin immunofluoresence of *Balaena mysticetus* and bovine retinae

B. mysticetus and bovine (*Bos taurus*) retinal cross-sections immunolabled with antisera against rhodopsin (red) and cone opsin (green). Nuclei are labeled with DAPI (blue). **A–C**: Outer segments of *B. mysticetus* retina labeled with anti-rhodopsin. Two distinct polyclonal long-wavelength sensitive (LWS) cone opsin antibodies (LWS^1 and LWS^2) and one polyclonal short-wavelength sensitive (SWS) cone opsin antibody failed to label the *B. mysticetus* retina. **D–F:** For comparison, both rhodopsin and cone opsin-expressing outer segments were labeled in the bovine retina. Scale bars indicate 10 μm.

Figure 2. Light and transmission electron microscopy of *Balaena mysticetus* and bovine photoreceptors

A: *B. mysticetus* retina contains a uniform layer of rod outer segments (ROS; arrowhead). **B:** Bovine retina contains morphologically distinct ROS and cone outer segments (COS; arrowheads). **C–D:** Transmission electron microscopy (TEM) reveals the ultrastructure of *B. mysticetus* photoreceptors to be characteristic of rods; **C:** Rods exhibit outer segments (black arrow) of a greater diameter than inner segments (**D**; white arrow). Cone outer segments and inner segments appear absent in the *B. mysticetus* retina. **E–F:** Bovine cone (**E**) and rod cells (**F**) exhibit the characteristic outer segment (black arrows) and inner segment (white arrows) morphologies of mammalian photoreceptors. Scale bars indicate 10 μm in A, B; 0.5 μm in C-F.

Figure 3: Light and transmission electron microscopy of *Balaena mysticetus* rod and cone somata and synapses

A–C: Light microscopy of the *B. mysticetus* retina. **A:** Rod (RN arrowhead) and cone nuclei (CN arrowheads) are observed, as well as rod spherules (black arrows) and putative cone pedicles (white arrow). **B:** A putative cone pedicle (white arrow) proximal to the nucleus of a horizontal cell. **C:** The retinal layers of *B. mysticetus* in a region of a putative cone pedicle (white arrow). **D–F:** Transmission electron microscopy of the *B. mysticetus* retina; cone nuclei (CN arrowhead), rod nuclei (RN arrowheads), rod spherules (black arrows) and putative cone pedicles (white arrows) were identified. Retinal layers are indicated: outer nuclear layer (ONL), outer plexiform layer (OPL), inner nuclear layer (INL), inner plexiform layer (IPL), ganglion cell layer (GCL). Scale bars indicate 10 μm in A–C; 1 μm in D–F.

Figure 4. Immunofluorescence labeling of rod and cone bipolar cells in *Balaena mysticetus*

A: Immunolabeling of protein kinase-C alpha (PKCα) demonstrates rod bipolar cells in the *B. mysticetus* retina. Immunolabeling of axonal ends adjacent to the ganglion cell layer (open arrow) is indicative of rod bipolar cells, while immunolabeling in the center of the inner plexifrom layer (IPL; solid arrow) suggests bistratified input of rod bipolar cell to the IPL. **B:** Anti-recoverin immunolabeling of cone bipolar cells in the outer half (white arrow) and inner half (open arrow) of the IPL indicate OFF- and ON-cone bipolar cells, respectively. **C:** Immunolabeling of anti-PKCα demonstrates rod bipolar cells in *B. mysticetus*. **D, E:** Anti-recoverin immunolabeling demonstrates OFF- and ON-cone bipolar cells respectively. Cell somata (CS) and cell termini (CT) are indicated by arrows. Retinal layers are indicated: outer nuclear layer (ONL), inner nuclear layer (INL), inner plexiform layer (IPL), ganglion cell layer (GCL). Scale bars indicate 10 μm.

Figure 5. Proposed functional architecture of the *Balaena mysticetus* retina

Cone somata and pedicles may have been conserved to maintain an alternative rod photoreceptor signaling pathway. Three distinct rod signaling pathways may increase the sensitivity range of rod-based vision in balaenid whales. **1:** The classical, most light sensitive, rod pathway; **2:** the rod-cone coupling pathway capable of operating at intermediate light (i.e., mesopic) levels; **3:** the cone bipolar cell pathway which may support important visual processes of rod-based vision. Red arrows indicate synaptic information flow; yellow ovals indicate gap junctions. Retinal layers are indicated: outer nuclear layer (ONL), inner nuclear layer (INL), inner plexiform layer (IPL), ganglion cell layer (GCL). Retinal cell types are indicated: rod (R), cone (C), rod bipolar cell (RBC), ON and OFF cone bipolar cells (CBC), AII type amacrine cell (AII), ON or OFF retinal ganglion cell (RGC).

Table 1. Primary and Secondary Antisera for Immunofluorescence

Antibody Name	Manufacturer	Catalog #	Immunogen	Host and Clonality	RRID	Dilution
Primary Antisera						
Anti-Rhodopsin	EMD Millipore	MAB5316	Membrane preparation from adult rat retina	Mouse Monoclonal	AB_2156055	1:500
Anti-Opsin, Red	W.J. DeGrip; U. Nijmegen, Netherlands	CERN906	Chicken LWS cone opsin	Rabbit Polyclonal	n/a	1:1000
Anti-Cone Opsin	W.J. DeGrip; U. Nijmegen, Netherlands	CERN874	Chicken cone opsin	Rabbit Polyclonal	n/a	1:4000
Anti-Opsin, Blue	EMD Millipore	AB5407	Recombinant human blue opsin	Rabbit Polyclonal	AB_177457	1:1000
Anti-PKC Alpha	Abcam	AB4127	Synthetic peptide: FEKAKLGPAGNKVISPEDRKQ; corresponding to amino acids 305-325 of Human PKC alpha.	Rabbit Polyclonal	AB_304300	1:200
Anti-Recoverin	EMD Millipore	AB5585	Recombinant human recoverin	Rabbit Polyclonal	AB_2253622	1:500
Secondary Antisera						
Goat anti-rabbit IgG (H&L), Alexa-Fluor 555 conjugated	Invitrogen	A21424	Mouse gamma immunoglobulin heavy and light chains	Goat Polyclonal	AB_141780	1:500
Goat anti-rabbit IgG (H&L), Alexa-Fluor 488 conjugated	Invitrogen	A11008	Rabbit, gamma immunoglobulin heavy and light chains	Goat Polyclonal	AB_143165	1:500

Table 2. Photoreceptor Outer Segment Number derived from Immunofluorescence (IF) and Light Microscopy (LM)

Retinal Tissue	Photoreceptor Type	IF Number/25µm ± SE	n	LM Number/25µm ± SE	n
B. mysticetus	Rod	11.50 ± 0.32	21	11.67 ± .33	8
B. mysticetus	LWS Cone	0 ± 0.0	21	0 ± 0.0	8
B. mysticetus	SWS Cone	0 ± 0.0	21	0 ± 0.0	8
Bos taurus	Rod	7.89 ± .59	50	7.56 ± 0.18	7
Bos taurus	LWS Cone	3.94 ± 0.12	50	-	-
Bos taurus	SWS Cone	1.88 ± 0.16	50	-	-
Bos taurus	All Cones	-	-	4.0 ± 0.24	7

Table 3. Bipolar cell type identification by positions of axon termini in the inner plexiform layer (IPL). Axon length is measured from the border between the inner nuclear layer (INL) and the IPL.

Retinal Tissue	n	IPL Thickness (µm ± SD)	Axon Length (µm ± SD)	Position of Axon Terminus in IPL	Bipolar Cell Type
B. mysticetus	2	32.56 ± 5.35	30.46 ± 6.36	Inner Half	Rod
B. mysticetus	3	46.93 ± 0.56	12.25 ± 0.99	Outer Half	OFF Cone
B. mysticetus	3	40.01 ± 0.56	25.53 ±0.99	Inner Half	ON Cone

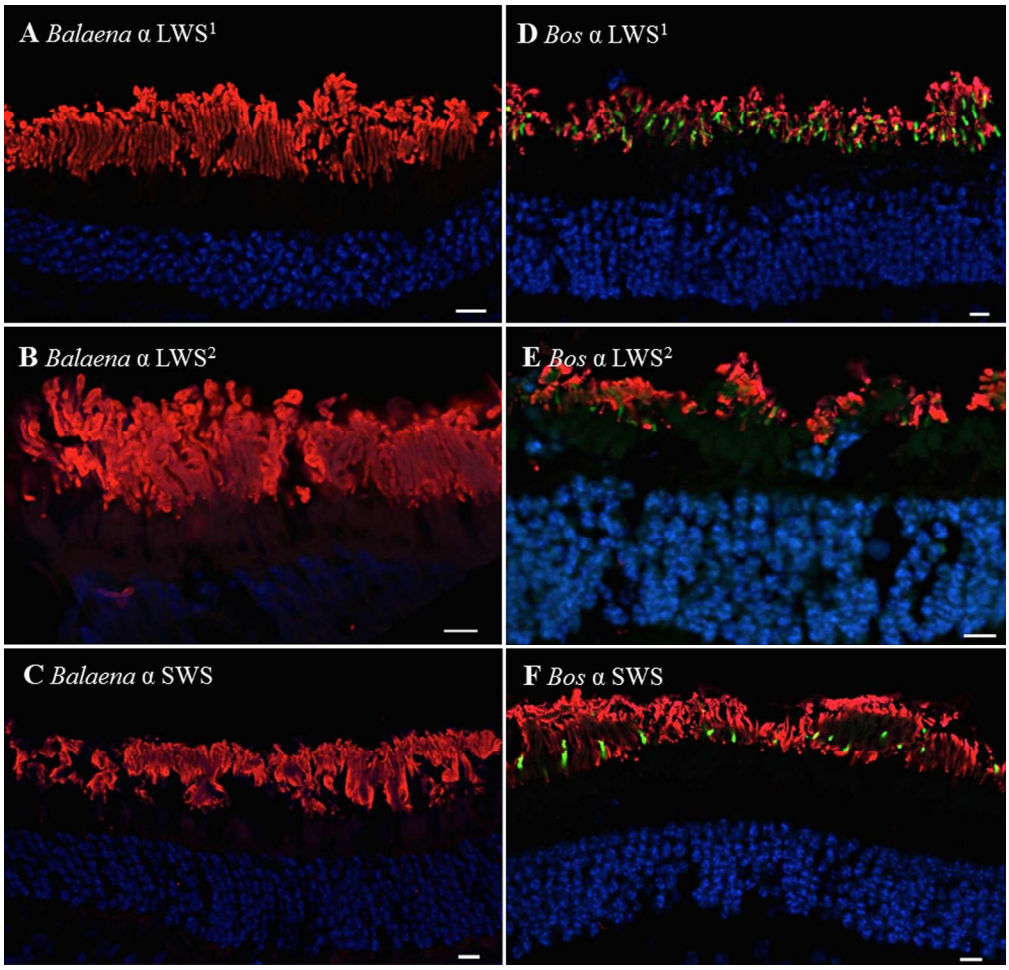

Figure 1. Anti-opsin immunofluoresence of *Balaena mysticetus* and bovine retinae

B. mysticetus and bovine (Bos taurus) retinal cross-sections immunolabled with antisera against rhodopsin (red) and cone opsin (green). Nuclei are labeled with DAPI (blue). A–C: Outer segments of *B. mysticetus* retina labeled with anti-rhodopsin. Two distinct polyclonal long-wavelength sensitive (LWS) cone opsin antibodies (LWS1 and LWS2) and one polyclonal short-wavelength sensitive (SWS) cone opsin antibody failed to label the *B. mysticetus* retina. D–F: For comparison, both rhodopsin and cone opsin-expressing outer segments were labeled in the bovine retina. Scale bars indicate 10 μm.
179x171mm (300 x 300 DPI)

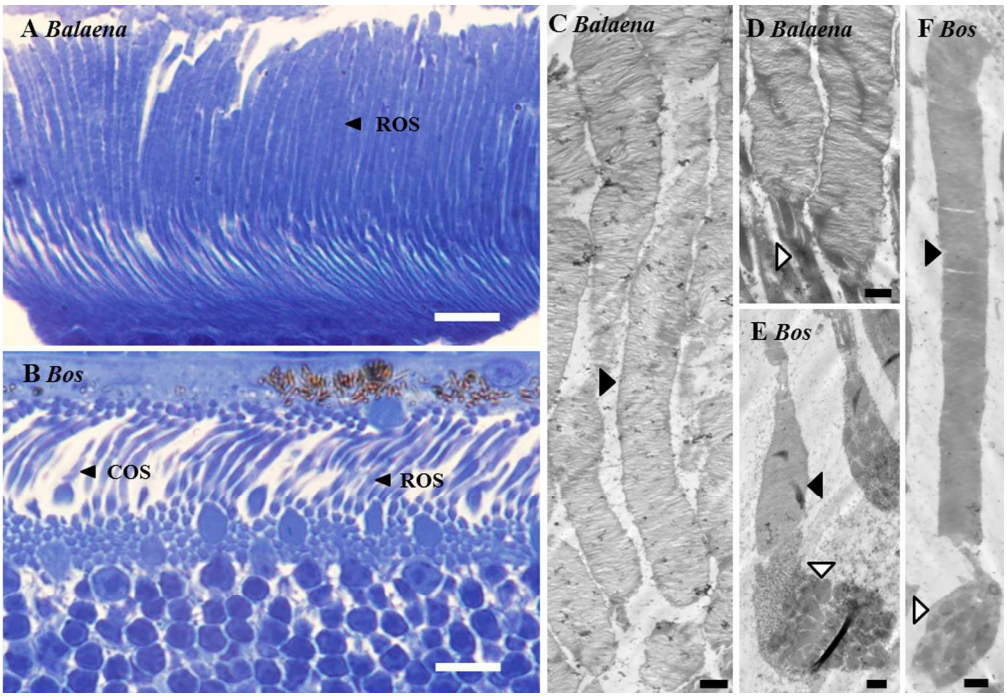

Figure 2. Light and transmission electron microscopy of *Balaena mysticetus* and bovine photoreceptors. A: *B. mysticetus* retina contains a uniform layer of rod outer segments (ROS; arrowhead). B: Bovine retina contains morphologically distinct ROS and cone outer segments (COS; arrowheads). C–D: Transmission electron microscopy (TEM) reveals the ultrastructure of *B. mysticetus* photoreceptors to be characteristic of rods; C: Rods exhibit outer segments (black arrow) of a greater diameter than inner segments (D; white arrow). Cone outer segments and inner segments appear absent in the *B. mysticetus* retina. E–F: Bovine cone (E) and rod cells (F) exhibit the characteristic outer segment (black arrows) and inner segment (white arrows) morphologies of mammalian photoreceptors. Scale bars indicate 10 μm in A, B; 0.5 μm in C-F.
250x171mm (300 x 300 DPI)

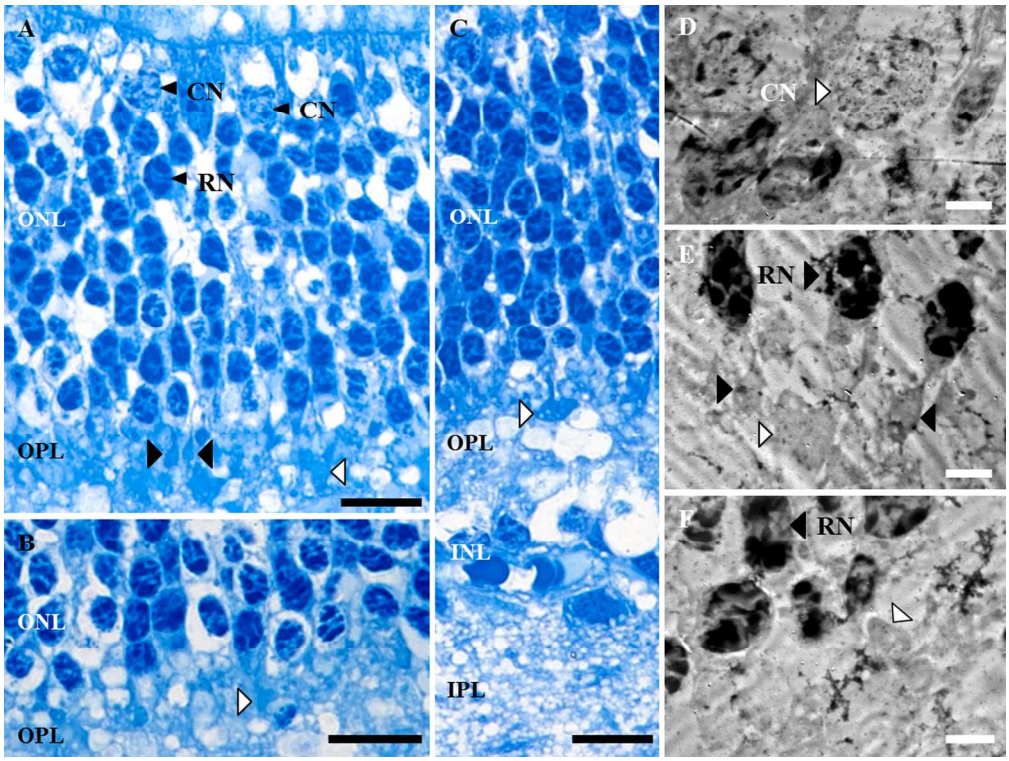

Figure 3: Light and transmission electron microscopy of *Balaena mysticetus* rod and cone somata and synapses.

A–C: Light microscopy of the *B. mysticetus* retina. A: Rod (RN arrowhead) and cone nuclei (CN arrowheads) are observed, as well as rod spherules (black arrows) and cone pedicles (white arrow). B: A presumptive cone pedicle (white arrow) proximal to the nucleus of a horizontal cell. C: The retinal layers of *B. mysticetus* in a region of a presumptive cone pedicle (white arrow). D–F: Transmission electron microscopy of the *B. mysticetus* retina; cone nuclei (CN arrowhead), rod nuclei (RN arrowheads), rod spherules (black arrows) and presumptive cone pedicles (white arrows) were identified. Retinal layers are indicated: outer nuclear layer (ONL), outer plexiform layer (OPL), inner nuclear layer (INL), inner plexiform layer (IPL), ganglion cell layer (GCL). Scale bars indicate 10 μm in A–C; 1 μm in D–F.
229x171mm (300 x 300 DPI)

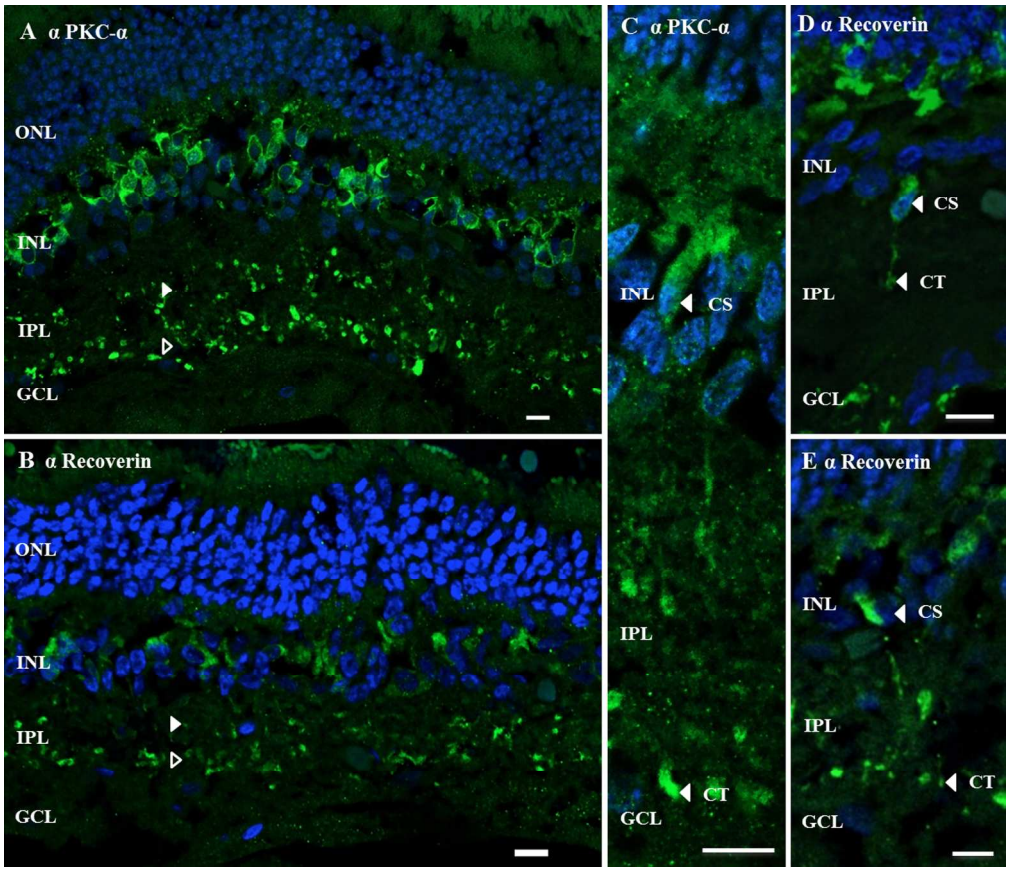

Figure 4. Immunofluorescence labeling of rod and cone bipolar cells in *Balaena mysticetus*.

A: Immunolabeling of protein kinase-C alpha (PKCα) demonstrates rod bipolar cells in the *B. mysticetus* retina. Immunolabeling of axonal ends adjacent to the ganglion cell layer (open arrow) is indicative of rod bipolar cells, while immunolabeling in the center of the inner plexifrom layer (IPL; solid arrow) suggests bistratified input of rod bipolar cell to the IPL. B: Anti-recoverin immunolabeling of cone bipolar cells in the outer half (white arrow) and inner half (open arrow) of the IPL indicate OFF- and ON-cone bipolar cells, respectively. C: Immunolabeling of anti-PKCα demonstrates rod bipolar cells in *B. mysticetus*. D, E: Anti-recoverin immunolabeling demonstrates OFF- and ON-cone bipolar cells respectively. Cell somata (CS) and cell termini (CT) are indicated by arrows. Retinal layers are indicated: outer nuclear layer (ONL), inner nuclear layer (INL), inner plexiform layer (IPL), ganglion cell layer (GCL). Scale bars indicate 10 μm.
199x171mm (300 x 300 DPI)

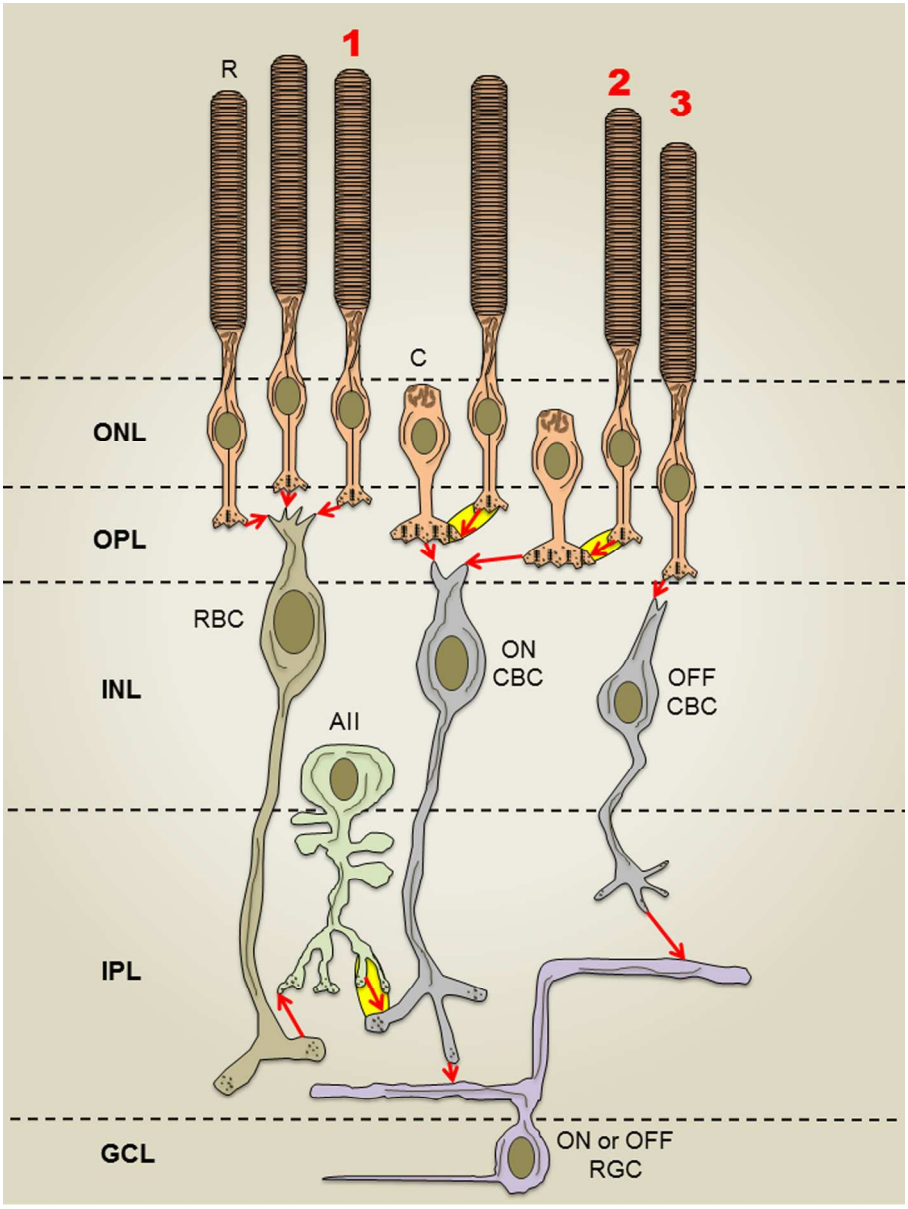

Figure 5. Proposed functional architecture of the *Balaena mysticetus* retina.

Cone somata and pedicles may have been conserved to maintain an alternative rod photoreceptor signaling pathway. Three distinct rod signaling pathways may increase the sensitivity range of rod-based vision in balaenid whales. 1: The classical, most light sensitive, rod pathway; 2: the rod-cone coupling pathway capable of operating at intermediate light (i.e., mesopic) levels; 3: the cone bipolar cell pathway which may support important visual processes of rod-based vision. Red arrows indicate synaptic information flow; yellow ovals indicate gap junctions. Retinal layers are indicated: outer nuclear layer (ONL), inner nuclear layer (INL), inner plexiform layer (IPL), ganglion cell layer (GCL). Retinal cell types are indicated: rod (R), cone (C), rod bipolar cell (RBC), ON and OFF cone bipolar cells (CBC), AII-type amacrine cell (AII), ON or OFF retinal ganglion cell (RGC).

129x171mm (300 x 300 DPI)

Using genetic sequencing along with immunofluorescence, light and electron microscopy, the authors show that baleen whales have experienced an evolutionary loss of cone photoreception in their retinas, yet they maintain important components of the cone-based light signaling pathway, perhaps to enhance the sensitivity range of their remaining rod-based vision.

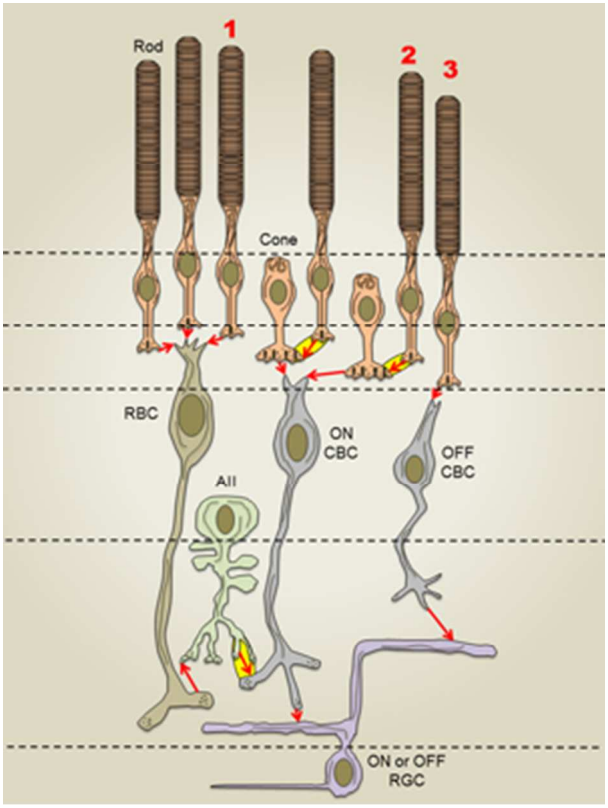

Graphical abstract image
105x141mm (72 x 72 DPI)